input port reflection $S_{11}$ at center design frequency $f_0$. In experiment, one circuit was fabricated, the results showed good agreement with simulated results.


## ACKNOWLEDGMENT

This work was supported by VLSI Design and Education Center (VDEC), the University of Tokyo in collaboration with Agilent Technologies Japan, Ltd. Chip capacitors were provided by the Murata Manufacturing Company Ltd., Kyoto, Japan. This work was financially supported by the Sasakawa Scientific Research Grant (No. 26-211) from the Japan Science Society.


## REFERENCES


1. E.J. Wilkinson, An N-way hybrid power divider, IRE Trans Microwave Theory Tech MTT 8 (1960), 116–118.
2. D. Pozar, Microwave engineering, Chapter 7, 3rd ed., Wiley, New York, 2005.
3. M.C. Scardelletti, G.E. Ponchak, and T.M. Weller, Miniaturized Wilkinson power dividers utilizing capacitive loading, IEEE Microwave Wireless Compon Lett 12 (2002), 6–8.
4. J. Li, S. Qu, and Q. Xue, Capacitively loaded Wilkinson power divider with size reduction and harmonic suppression, Microwave Opt Technol Lett 49 (2007), 2737–2739.
5. W.-C. Ip and K.-K.M. Cheng, A novel power divider design with enhanced harmonic suppression and simple layout, In: IEEE MTT-S International Microwave Symposium Digest, Anaheim, CA, May 2010, pp. 125–128.
6. A.R. Hazeri, A new miniaturization and the nth harmonic suppression of Wilkinson power, IEICE Trans Electron E94-C (2011), 215–219.
7. X. Tang and K. Mouthaan, Analysis and design of compact two-way Wilkinson power dividers using coupled lines, In: Proceedings of Asia-Pacific Microwave Conference, Singapore, December 2009, pp. 1319–1322.
8. Y. Wu, Y. Liu, and Q. Xue, An analytical approach for a novel coupled line dual-band Wilkinson power divider, IEEE Trans Microwave Theory Tech 59 (2011), 286–294.
9. M. Dydyk, Microstrip directional couplers with ideal performance via single-element compensation, IEEE Trans Microwave Theory Tech 47 (1999), 956–964.
10. J. Muller, M.N. Pham, and A.F. Jacob, Directional coupler compensation with optimally positioned capacitances, IEEE Trans Microwave Theory Tech 59 (2011), 2824–2832.
11. X. Wang, I. Sakagami, K. Takahashi, and S. Okamura, A generalized dual-band Wilkinson power divider with parallel L, C and R components, IEEE Trans Microwave Theory Tech 60 (2012), 952–964.




# WIDEBAND SUBSTRATE INTEGRATED WAVEGUIDE CAVITY-BACKED SPIRAL-SHAPED PATCH ANTENNA


**Longsheng Liu, Han Wang, Zhijun Zhang, Yue Li, and Zhenghe Feng**

State Key Lab of Microwave and Communications, Department of Electronic Engineering, Tsinghua University, Beijing 100084, China; Corresponding author: zjzh@tsinghua.edu.cn



*Received 25 June 2014*



**ABSTRACT:** *A new technique for designing wideband substrate integrated waveguide (SIW) cavity-backed antenna is presented in this article. The antenna element is composed of a spiral-shaped patch and an SIW cavity fed by a coaxial probe. It takes advantage of a dual-resonance observed in the proposed spiral-shaped patch structure to enhance its bandwidth. A 2 × 1 array is designed to increase the antenna gain. To demonstrate the validity of the bandwidth enhancement technique, prototypes of the proposed antenna element and array for X-band applications are fabricated and measured. The measure 10-dB return loss bandwidth of the antenna element is 11.2% (10.306–11.531 GHz) while that of the array is 12.5% (10.292–11.66 GHz).*

 Microwave Opt Technol Lett 57:332–337, 2015; View this article online at wileyonlinelibrary.com. DOI 10.1002/mop.28844

**Key words:** *substrate integrated waveguide; spiral-shaped patch, wideband; dual-resonance*

## 1. INTRODUCTION

Waveguide-fed slot antennas have been extensively investigated and widely applied for communication and radar systems owing to their attractive features of high directivity, high power handling, low cross-polarization levels, and accurate control capability of the radiation patterns [1].

In recent years, antennas with light weight, low cost, high performance, and high integration have gained increasing attention. In spite of all their advantages, traditional waveguide-fed slot antennas are costly, heavy, and bulky. To eliminate the aforementioned drawbacks, substrate integrated waveguide (SIW) was suggested as an alternative technology to facilitate the low-cost implementation of waveguide-like structure compatible with existing planar processing techniques such as printed circuit board (PCB) or low-temperature cofired ceramic [2]. During the past decades, SIW has experienced unprecedented development for its significant advantages, namely, low loss, low cost, low profile, high $Q$-factor, high power-handling capability, easiness of integration, and improved electromagnetic compatibility/electromagnetic interference shielding with self-consistent electromagnetic shielding [3]. However, antennas based on SIW suffer from limited bandwidths usually around 3% or less because of their low profile and dielectric filling effect [4].

Recently, various techniques have been proposed to enhance the bandwidth. A T-type folded SIW structure was proposed to design a 4 × 4 slot array antenna with a broadened bandwidth of 8.8% [5]. An SIW slot array with center-fed technique demonstrated a measured bandwidth of 9.8% [6]. Minkowski fractal geometry was proposed to design an SIW slot array with an enhanced bandwidth up to 12.1% [7]. An SIW slotted narrow-wall fed cavity antennas was designed for millimeter-wave, in which the inductive window along with the inductive via behaving as a T-shape network enhanced the bandwidth to about 13% [8]. A millimeter wave cavity-backed patch antenna and array based on $TE_{210}$ mode SIW were proposed, where the coupling between the adjacent $TE_{210}$ mode of SIW cavity and $TM_{10}$ mode of the patch antenna improved the bandwidth of the single element to 15.6% and that of a 4 × 4 array to 8.7% [9].

Different from the aforementioned methods [5–9], an SIW cavity-backed spiral-shaped patch antenna and a 2 × 1 array are presented in this article. The antenna element is formed by etching a spiral slot on the upper metal layer of the traditional SIW cavity. Together with the spiral slot, the inner spiral-shaped patch structure demonstrates wideband performance with dual resonation.

This article is organized as follows. In Section 2, the antenna element as well as a 2 × 1 array is introduced, wherein the operation mechanism of the antenna element is explored. Parametric study is performed to verify the dual-resonance behavior of the antenna element in Section 3. Prototypes of the proposed

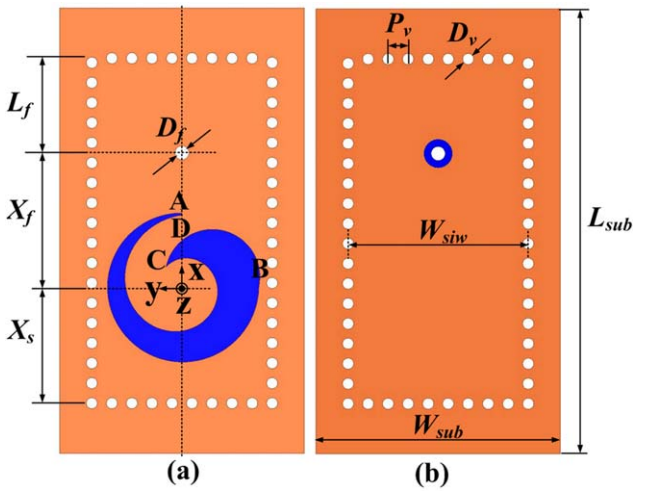


**Figure 1** Geometry of the proposed antenna element ($W_{sub} = 22$, $L_{sub} = 40$, $W_{SIW} = 16.2$, $P_v = 1.8$, $D_v = 1$, $X_s = 10.5$, $L_f = 8.5$, $X_f = 12$, $D_f = 1.27$, $A_1 = 6.6$, $A_2 = 6.4$, $R_1 = 0.01$, $R_2 = -0.15$, $\varphi_1 = 270$, $\varphi_2 = 400$, all values are in millimetres except that $\varphi_1$, $\varphi_2$ are in degree and $R_1$, $R_2$ are dimensionless). (a) Top view and (b) bottom view. [Color figure can be viewed in the online issue, which is available at wileyonlinelibrary.com]

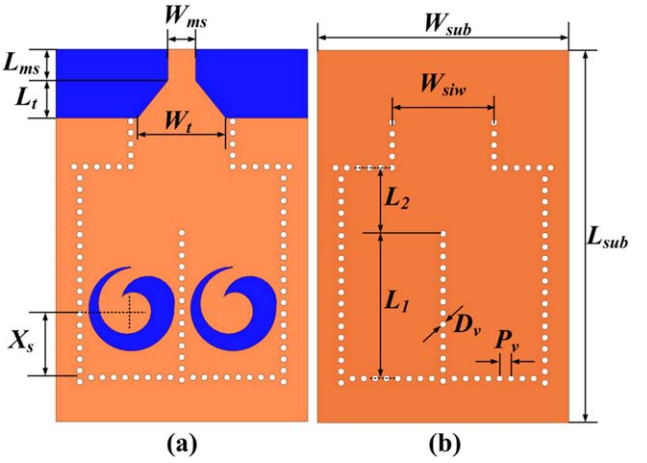


**Figure 3** Geometry of the proposed 2 × 1 array ($W_{sub} = 40$, $L_{sub} = 59.2$, $W_{siw} = 16.2$, $P_v = 1.8$, $D_v = 1$, $L_1 = 23$, $L_2 = 10.5$, $X_s = 11$, $W_t = 14$, $L_t = 6$, $W_{ms} = 4.34$, $L_{ms} = 5$, all values are in millimetres). (a) top view and (b) bottom view. [Color figure can be viewed in the online issue, which is available at wileyonlinelibrary.com]

antenna element and 2 × 1 array at X-band are fabricated to experimentally validate the analysis and concepts with their simulated and experimental results shown in Section 4, and some conclusion will be drawn in the end.

## 2. ANTENNA DESIGN

The geometric structure of the antenna element is illustrated in Figure 1. The antenna is simulated and optimized with the aid of ANSYS HFSS. The used substrates for the proposed element and array are F4B with a relative dielectric constant of 2.55 and a thickness of 1.50 mm. As can be seen from Figure 1, the presented antenna element is formed by etching a spiral-shaped slot on the upper metal layer of the traditional SIW cavity which is excited by a coaxial probe. The spiral-shaped slot without the SIW cavity is similar to that introduced in [10]. The dimensions and operating mechanism are quite different, where the travelling surface currents propagating along the curved slot are applied for achieving wideband circularly polarized radiation in [10]. However, with the loading of the low profile SIW cavity in our design, the electric field fails to establish across the spiral-shaped slot owing to the width of the spiral-shaped slot is so large compared with the thickness of the SIW cavity. The radiation is principally contributed by the inner spiral-shaped patch; while the impedance matching is improved by the tapered spiral-shaped slot.

The propagation constant and the radiation loss of SIW are determined by parameters $W_{SIW}$, $D_v$, and $P_v$, which denote the width of the SIW, the diameter and the period of vias, respectively. Owing to the similar propagation characteristics between SIW and rectangular waveguide, SIW can be equivalent to a dielectric-filled rectangular waveguide with a width of $a_{rwg}$ and the same height of $h$ [11]. It is desirable to design the SIW resonating between the cutoff frequencies of $TE_{10}$ and $TE_{20}$ modes which can be calculated by the equations in [11,12].

The spiral-shaped slot in Figure 1 is formed by two exponential curves $L_1$ (A to B) and $L_2$ (D to C) terminated with a semicircular arc $L_3$ (B to C). The curves $L_1$ and $L_2$ are determined by the following equations in Cartesian coordinates:

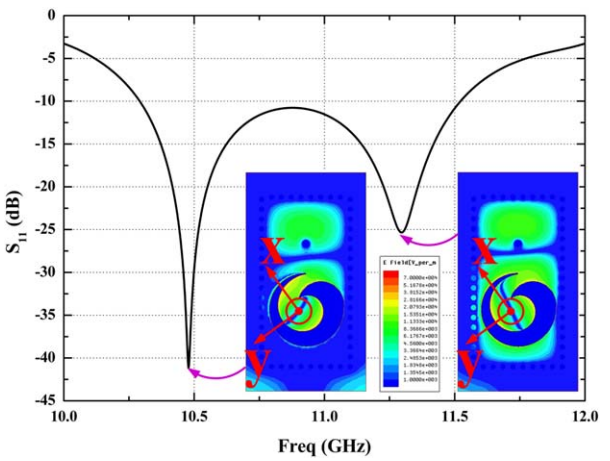


**Figure 2** Simulated $S_{11}$ of the proposed antenna element and the electric field distribution of the resonances. [Color figure can be viewed in the online issue, which is available at wileyonlinelibrary.com]

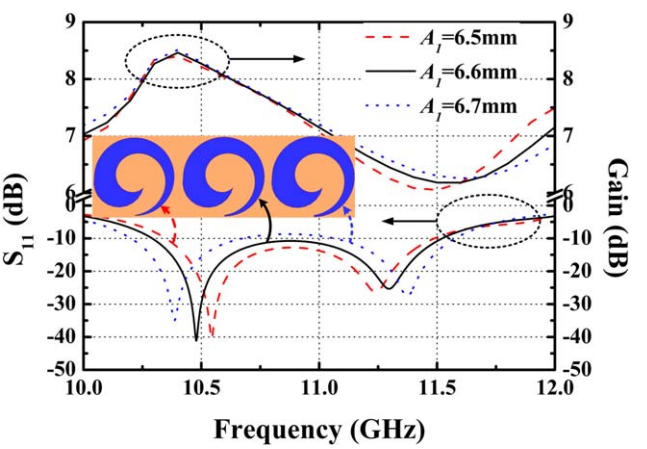


**Figure 4** Effect of $A_1$ on $S_{11}$ and gain. [Color figure can be viewed in the online issue, which is available at wileyonlinelibrary.com]

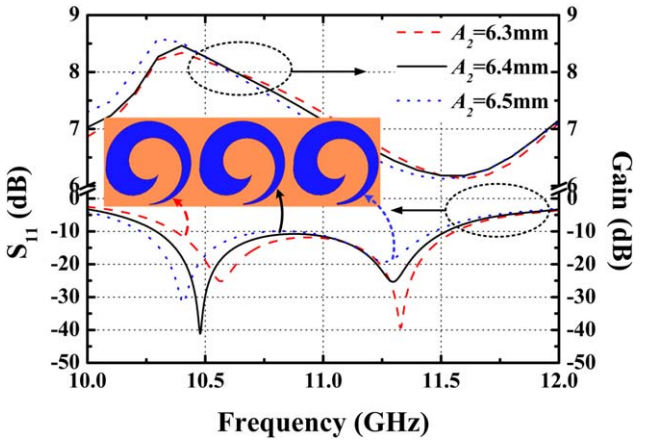


**Figure 5** Effect of $A_2$ on $S_{11}$ and gain. [Color figure can be viewed in the online issue, which is available at wileyonlinelibrary.com]

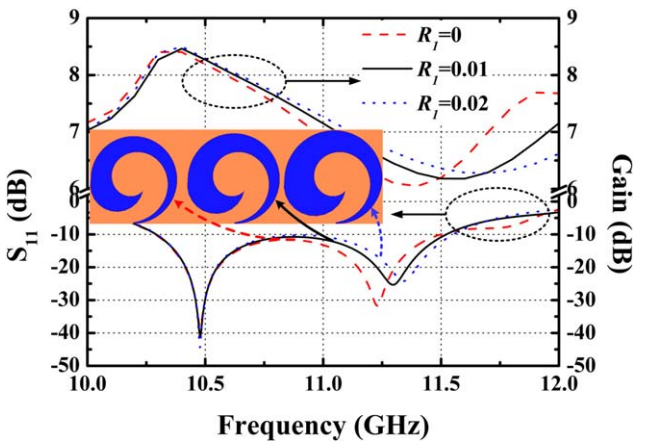


**Figure 6** Effect of $R_1$ on $S_{11}$ and gain. [Color figure can be viewed in the online issue, which is available at wileyonlinelibrary.com]

$$L_i: \begin{cases} x = A_i\ e^{R_i\varphi}\cos(\varphi) \\ y = A_i\ e^{R_i\varphi}\sin(\varphi) \\ z = 0 \end{cases} \quad \text{with } \varphi = [0,\ \varphi_i],\ \text{i} = 1,\ 2 \quad (2)$$

Where $A_i$ is the initial radius of the $i$th exponential curve with respect to the origin of Cartesian coordinates shown in Figure 1; $R_i$ and $\varphi_i$ are the growing rate and the stop angle of the $i$th exponential curve, respectively.

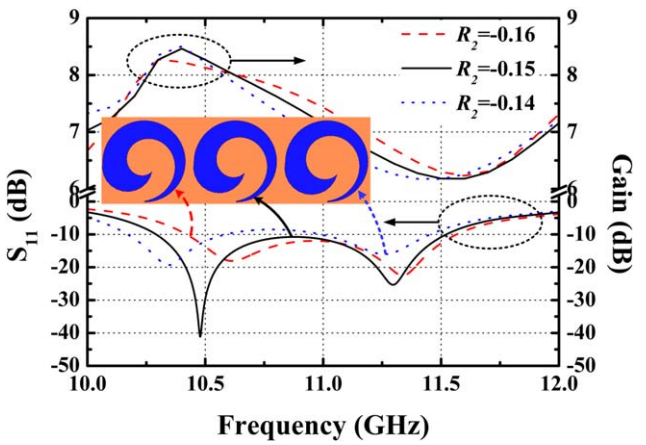


**Figure 7** Effect of $R_2$ on $S_{11}$ and gain. [Color figure can be viewed in the online issue, which is available at wileyonlinelibrary.com]

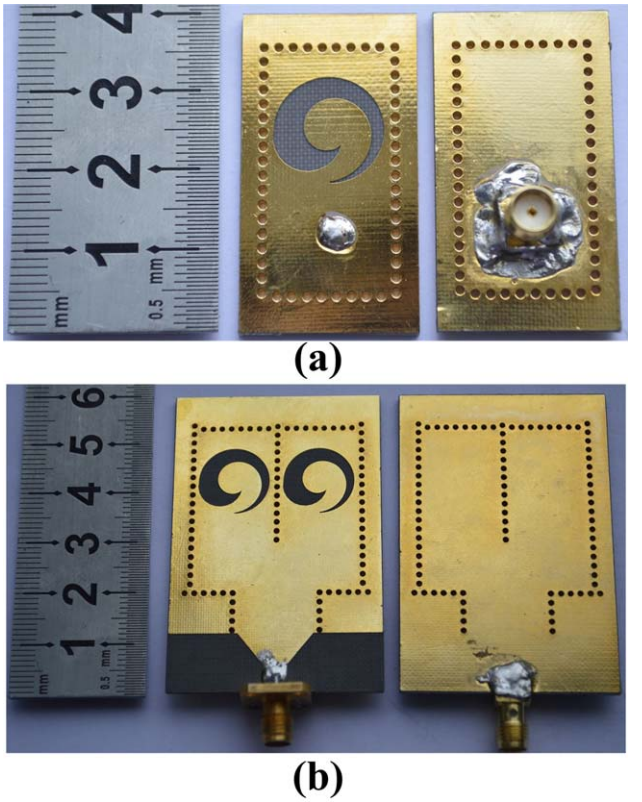


**Figure 8** Photograph of the fabricated prototypes. (a) the antenna element and (b) the 2 × 1 array. [Color figure can be viewed in the online issue, which is available at wileyonlinelibrary.com]

The operation of the proposed antenna element mainly rests on the radiation from the inner spiral-shaped patch. Dual resonances can be observed from the simulated reflection coefficient represented in Figure 2. To understand the operating principle, the insets of Figure 2 depict the electric field distributions over the upper aperture at resonant frequencies of 10.48 and 11.313 GHz, which determine the radiation performance of the proposed element. At 10.48 GHz, the electric field is maximum at the two ends of the spiral-shaped patch and minimum approximately in the center, which is similar to that of a microstrip patch antenna resonating at mode $TM_{10}$ in the relative

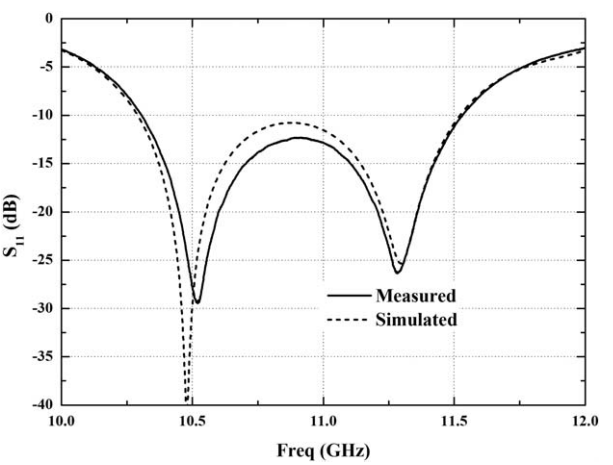


**Figure 9** Simulated and measured $S_{11}$ of the antenna element

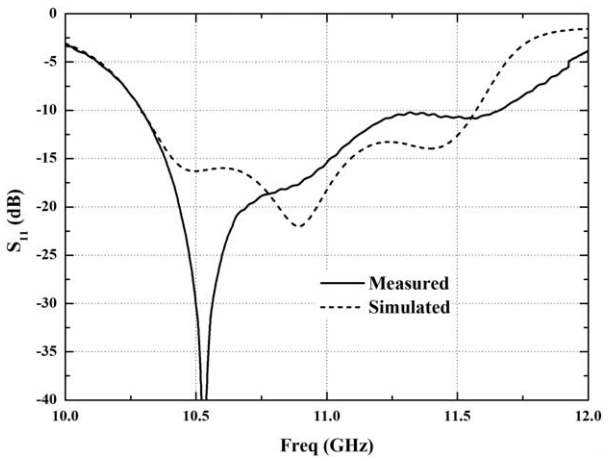


**Figure 10** Simulated and measured $S_{11}$ of the 2 × 1 array

coordinates system shown in the left inset, likewise, the electric field at 11.313 GHz reveals a $TM_{01}$ mode as shown in the right inset.

To increase the gain, A 2 × 1 array are designed. As shown in Figure 3, the proposed 2 × 1 array is composed of two elements placed side by side, a Y-junction power divider based on SIW [13], and a microstrip-to-SIW transition. The transition is used to transform the quasi-TEM mode of the microstrip line into the $TE_{10}$ mode in SIW structure [14].

## 3. PARAMETRIC STUDY OF THE ANTENNA ELEMENT

As shown in Figures 4–7, the antenna's impedance matching characteristics is significantly affected by the spiral slot while the resonate frequencies and the gain are mainly determined by the inner spiral-shaped patch.

### *3.1. Effects of Initial Radius $A_1$ and $A_2$*

Figures 4 and 5 display the simulated reflection coefficient and gain with different $A_1$ and $A_2$. The spiral-shaped patch remains unchanged while the spiral slot is enlarged with the increase of $A_1$. Therefore, impedance matching and bandwidth can be improved by varying $A_1$ whereas the gain is insensitive to $A_1$ variation. However, the size of the spiral patch becomes larger as $A_2$ increases, therefore, both the two resonant frequencies and the peak gain shift downward.

### *3.2. Effects of Growing Rate $R_1$ and $R_2$*

The influences of $R_1$ and $R_2$ on the reflection coefficient and gain are depicted in Figures 6 and 7, respectively. As $R_1$ increases, the lower resonate frequency remains the same owing to the fact that the spiral-shaped patch keeps unchanged while the higher resonate frequency shifts upward with the enlarged spiral slot. The size of the spiral patch becomes larger with the increase of $R_2$, therefore, both the two resonant frequencies and the peak gain shift downwards. However, the two resonant frequencies begin to separate from each other by further increasing $R_2$ from −0.15 to −0.14.

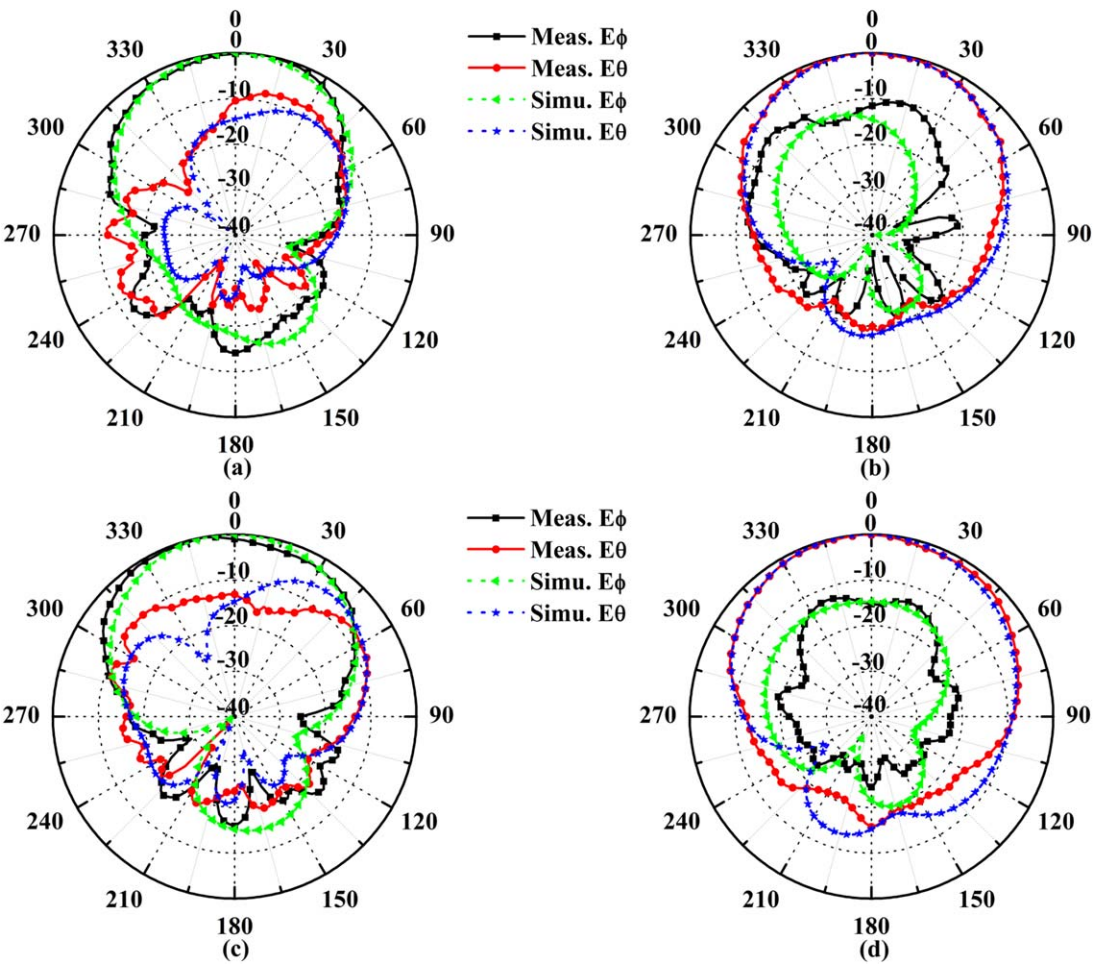


**Figure 11** Simulated and measured normalized radiation patterns of the antenna element. (a) *xz*-plane at 10.5 GHz; (b) *yz*-plane at 10.5 GHz; (c) *xz*-plane at 11 GHz; and (d) *yz*-plane at 11 GHz. [Color figure can be viewed in the online issue, which is available at wileyonlinelibrary.com]

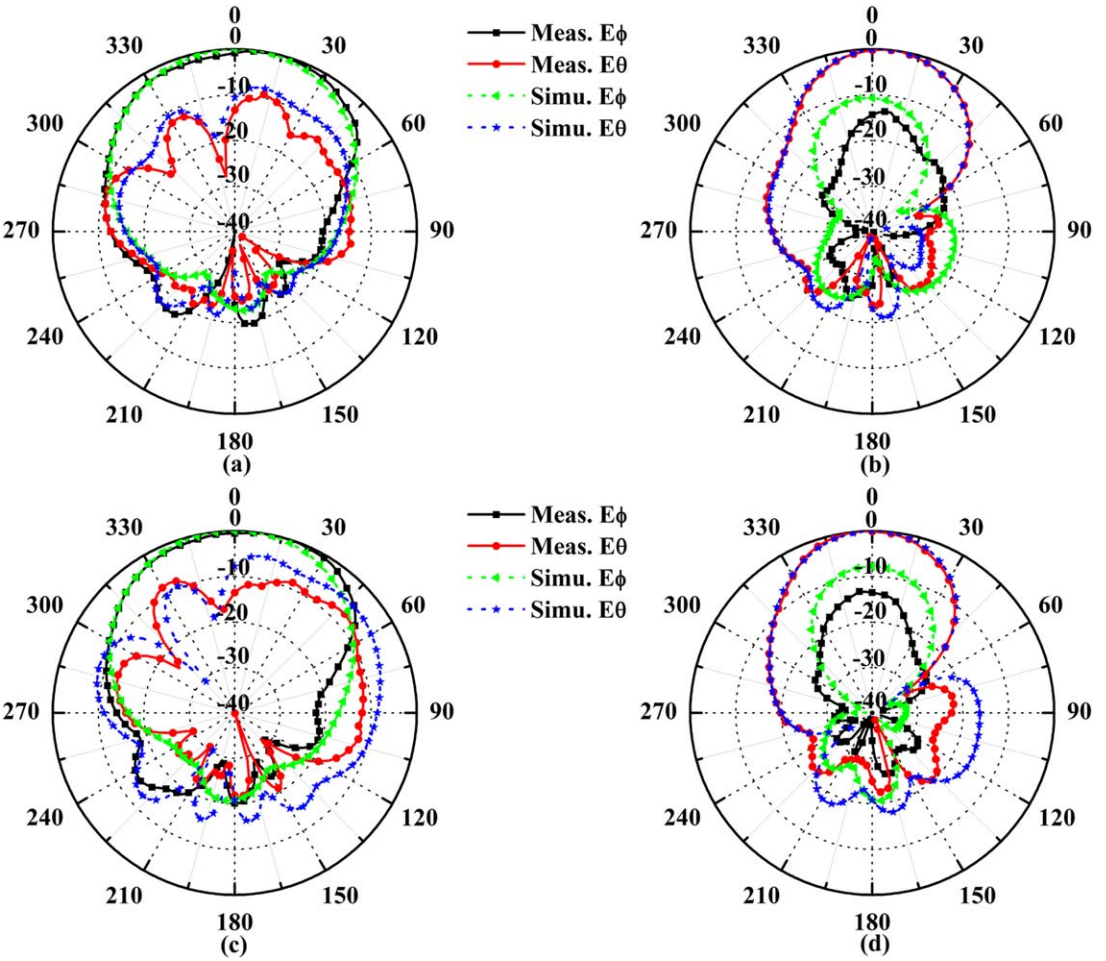


**Figure 12** Simulated and measured normalized radiation patterns of the 2 × 1 array. (a) *xz*-plane at 10.5 GHz; (b) *yz*-plane at 10.5 GHz; (c) *xz*-plane at 11 GHz; and (d) *yz*-plane at 11 GHz. [Color figure can be viewed in the online issue, which is available at wileyonlinelibrary.com]

## 4. RESULTS AND DISCUSSION

To demonstrate the validity of the presented design strategy, as shown in Figure 8, prototypes of the element and the 2 × 1 array were fabricated and measured. Simulated and measured results are given in Figures 9–14. Reasonable agreement between them could be observed.

### *4.1. S-parameter*

The reflection coefficients were measured by Agilent E8363B vector network analyzer. Figure 9 shows that the simulated and measured impedance bandwidth ($S_{11} < -10$ dB) of the antenna element are 11.3% (10.292–11.522 GHz) and 11.2% (10.306–11.531 GHz), respectively. The simulated impedance bandwidth ($S_{11} < -10$ dB) of the 2 × 1 array is 11.7% (10.292–11.571 GHz) while

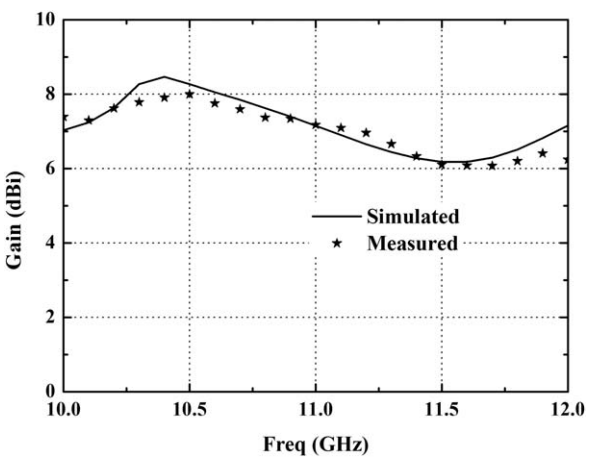


**Figure 13** Simulated and measured gain at broadside of the antenna element

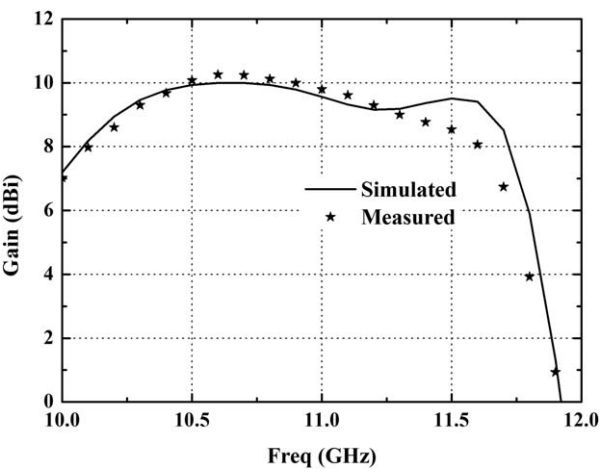


**Figure 14** Simulated and measured gain at broadside of the 2 × 1 array

the measured is 12.5% (10.292–11.66 GHz) as presented in Figure 10.

### 4.2. Radiation Pattern

The radiation patterns were measured in an anechoic chamber. Figures 11 and 12 show the simulated and measured normalized radiation patterns of the antenna element and the 2 × 1 array in both *xz*- and *yz*-plane at 10.5 and 11 GHz, respectively. As can be seen from Figures 11 and 12, both the element and the 2 × 1 array exhibit unidirectional patterns.

### 4.3. Antenna Gain

The simulated and measured gain at broadside of the antenna element and the 2 × 1 array are illustrated in Figures 13 and 14, respectively. The measure gain of the element ranges from 6 to 8 dBi whereas that of the 2 × 1 array is about 8–10 dBi over the impedance bandwidth. The discrepancies between the simulated and measured results may be caused by the fabrication error and measurement system setup.

## 5. CONCLUSION

A new method to enhance the impedance bandwidth of an SIW-based antenna is proposed and investigated in this article. The technique consists in exciting two different modes of a spiral-shaped patch structure. The parametric study has been performed to verify the dual-resonance behavior of the antenna. The fabricated prototypes exhibit good impedance bandwidth of 11.2 and 12.5% for the antenna element and 2 × 1 array, respectively. The proposed antenna has the advantages of wideband, low cost, and good integration ability, which makes it a suitable candidate for X-band applications using a standard PCB process.


## ACKNOWLEDGMENT

This work is supported by the National Basic Research Program of China under Contract 2013CB329002, in part by the National High Technology Research and Development Program of China (863 Program) under Contract 2011AA010202, the National Natural Science Foundation of China under Contract 61271135, the National Science and Technology Major Project of the Ministry of Science and Technology of China 2013ZX03003008-002.


## REFERENCE


1. G. Ruggerini, An X-band slotted waveguide array for radar applications, In: IEEE Proceedings of the 5th European Conference on Antennas and Propagation (EuCAP), Rome, 2011, pp. 1912–1914.
2. D. Deslandes and K. Wu, Accurate modeling, wave mechanisms, and design considerations of a substrate integrated waveguide, IEEE Trans Microwave Theory Tech 54 (2006), 2516–2526.
3. M. Bozzi, A. Georgiadis, and K. Wu, Review of substrate-integrated waveguide circuits and antennas, IET Microwave Antennas Propag 5 (2011), 909–920.
4. K. Gong, Z.N. Chen, X.M. Qing, P. Chen, and W. Hong, Substrate integrated waveguide cavity- backed wide slot antenna for 60-GHz bands, IEEE Trans Antennas Propag 60 (2012), 6023–6026.
5. Y. Ding and K. Wu, A 4×4 ridge substrate integrated waveguide (RSIW) slot array antenna, IEEE Antennas Wireless Propag Lett 8 (2009), 561–564.
6. M. Chen and W.Q. Che, Bandwidth enhancement of substrate integrated waveguide (SIW) slot antenna with center-fed techniques, In: 2011 International Workshop on Antenna Technology (iWAT), Hong Kong, 2011, pp. 348–351.
7. H.S. Farahani, A.K.-Salmani, M. Tayarani, R.A. Sadeghzadeh, and S. Chamaani, A novel approach for bandwidth enhancement of SIW-based slot array antenna, In: IEEE Proceedings of the 6th European Conference on Antennas and Propagation (EuCAP), Prague, 2012, pp. 1–3.
8. Y. Zhang, K. Gong, Z.N. Chen, X.M. Qing, and W. Hong, Wideband millimeter-wave substrate integrated waveguide slotted narrow-wall fed cavity antennas, IEEE Trans Antennas Propag 59 (2011), 1488–1496.
9. T.Y. Yang, W. Hong, and Y. Zhang, Wideband millimeter-wave substrate integrated waveguide cavity-backed rectangular patch antenna, IEEE Antennas Wireless Propag Lett 13 (2014), 205–208.
10. S.-K. Lin, Y.-C. Lin, A compact outer-fed leaky-wave antenna using exponentially tapered slots for broadside circularly polarized radiation, IEEE Trans Antennas Propag 60 (2012), 2654–2661.
11. L. Yan, W. Hong, and K. Wu, T.J. Cui, Investigations on the propagation characteristics of the substrate integrated waveguide based on the method of lines, IEE Proc Microwave Antennas Propag 152 (2005), 35–42.
12. K. Ogusu, Numerical analysis of the rectangular dielectric waveguide and its modifications, IEEE Trans Microwave Theory Tech 11 (1977), 874–885.
13. S. Germain, D. Deslandes, and K. Wu, Development of substrate integrated waveguide power dividers, In: IEEE 2003 Canadian Conference on Electrical and Computer Engineering (CCECE), Montréal, 2003, pp. 1921–1924.
14. D. Deslandes and K. Wu, Integrated microstrip and rectangular waveguide in planar form, IEEE Microwave Wireless Compon Lett 11 (2001), 68–70.




# ESTIMATION OF RESONANT FREQUENCY AND BANDWIDTH OF COMPACT UNILATERAL COPLANAR WAVEGUIDE-FED FLAG SHAPED MONOPOLE ANTENNAS USING ARTIFICIAL NEURAL NETWORK


**N. Gunavathi and D. Sriramkumar**
National Institute of Technology, Tiruchirappalli, Tamil Nadu 15, India; Corresponding author: gunavathi@nitt.edu


*Received 30 June 2014*


**ABSTRACT:** *Neural network based estimation of resonant frequency and bandwidth of compact unilateral coplanar waveguide (CPW)-fed flag shaped printed monopole antennas is presented. The proposed antennas are similar to CPW-fed antenna; however, by replacing unilateral CPW feed instead of CPW feed, compactness of about 48.615 percent is achieved. These are designed on an inexpensive FR4-epoxy substrate with dielectric constant of 4.4 and thickness of 1.6 mm. Resonant frequencies and bandwidths of the flag shaped antennas with different dimensions are computed using method of moment electromagnetic solver IE3D 15.10 and they have been given as training and test data for the proposed multilayered perceptron feed forward neural network with Levenberg–Marquardt training algorithm to estimate the resonant frequency and bandwidth of the proposed antennas. The estimated values of resonant frequency and bandwidth with average percentage of error are 1.275 and 0.325, respectively. For verification, the proposed antenna is fabricated and measured with resonant frequency 5.78 GHz and bandwidth of 1.0 GHz for HiperLAN/2 and IEEE802.11a applications. It has impedance bandwidth from 5.0 to 6.0 GHz for return loss lower than −10 dB and good omnidirectional radiation performance over entire frequency range, with a compact size of 11.07 × 27.5 × 1.6 mm$^3$. Various features such as compactness, simple geometry, and low cost, uniplanar structure make the antennas suitable for modern wireless communication systems. This approach replaces the use of very complicated analysis.* © 2015 Wiley Periodicals, Inc. Microwave Opt Technol Lett 57:337–342, 2015; View this article online at wileyonlinelibrary.com. DOI 10.1002/mop.28838


**Key words:** *5-GHz WLAN; ANN; antenna; compact; monopole; HIPERLAN/2; Levenberg–Marquardt algorithm; IEEE802. 11a; unilateral; uniplanar*